Helical network model for twisted bilayer graphene

Dmitry K. Efimkin and Allan H. MacDonald

The Center for Complex Quantum Systems, The University of Texas at Austin, Austin, Texas 78712-1192, USA

In the presence of a finite interlayer displacement field, bilayer graphene has an energy gap that is dependent on stacking and largest for the stable AB and BA stacking arrangements. When the relative orientations between layers are twisted through a small angle to form a moiré pattern, the local stacking arrangement changes slowly. We show that for nonzero displacement fields the low-energy physics of twisted bilayers is captured by a phenomenological helical network model that describes electrons localized on domain walls separating regions with approximate AB and BA stacking. The network band structure is gapless and has of a series of two-dimensional bands with Dirac band-touching points and a density of states that is periodic in energy with one zero and one divergence per period.

I. INTRODUCTION

The electronic structure of bilayer graphene is sensitive to strain, interlayer potential differences, and the stacking arrangement between layers [1,2]. For the energetically favored Bernal stacking configurations, either AB or BA, Bloch states have 2π Berry phases, quadratic band touchng, and a gap that opens when a displacement field is applied by external gates. The gapped state is characterized by nontrivial valley-dependent Chern numbers and supports topological confinement of electrons on domain walls that separate regions with opposite signs of displacement field [3–6] or different stacking arrangements [7–9]. The presence of confined electronic states, which occur in helical pairs with opposite propagation directions in opposite valleys, has [10–12] been confirmed experimentally. Control of these domain walls and of their intersections has attracted attention recently [13–18] because of its potential relevance for valleytronics [19].

While engineering of a network of helical states with tunable geometry is a challenging problem, the network of helical domain wall states localized on the links of a triangular lattice expected in misoriented graphene bilayers [20–41] has, in fact, been observed very recently [42]. In the presence of a twist, the local stacking arrangement changes slowly in space in a periodic moiré pattern in which regions with approximate AB and BA stacking are separated by domain walls with helical states. The measured local density of states at a domain wall is strongly energy dependent with a single peak within the gap that demonstrates the importance of an interference between helical states propagating along the network. Because the moiré pattern is well developed only when its period greatly exceeds graphene's lattice constant, theories of its electronic structure [43,44] often employ complicated multiscale approaches to advantage.

In this paper, we derive a phenomenological helical network model for the electronic structure of gated bilayer graphene moirés valid in the energy range below the AB and BA gaps where only topologically confined domain wall states are present. The model is related to Chalker-Coddington-type models [45–47] introduced in theories of the quantum Hall effect. The spectrum of the network model consists of a set

of minibands connected by Dirac band-touching points, which repeats and is gapless. A single period of the model's band structure is illustrated in Fig. 1.

II. DOMAIN WALL NETWORK

To describe the electronic structure of gated bilayer graphene with a small twist angle $\theta \lesssim 1°$ [48] between layers, we start from the continuum model Hamiltonian derived in Ref. [20], which is valid independent of atomic scale commensurability

$$H_0 = \begin{pmatrix} v\sigma_t \mathbf{p} - u & T(\mathbf{r}) \\ T^+(\mathbf{r}) & v\sigma_b \mathbf{p} + u \end{pmatrix}. \tag{1}$$

The Hamiltonian for a valley K acts in the sublattice space $\psi = \{\psi_A^t, \psi_B^t, \psi_A^b, \psi_B^b\}$, where t and b refer to the top and bottom layer and v is the single-layer Dirac velocity; $\sigma_{t(b)}$ is the vector of Pauli matrices rotated by the angle $\pm\theta/2$ in the top and bottom layers, and $2u$ is the potential difference between layers produced by the gates. The spectrum is valley and spin
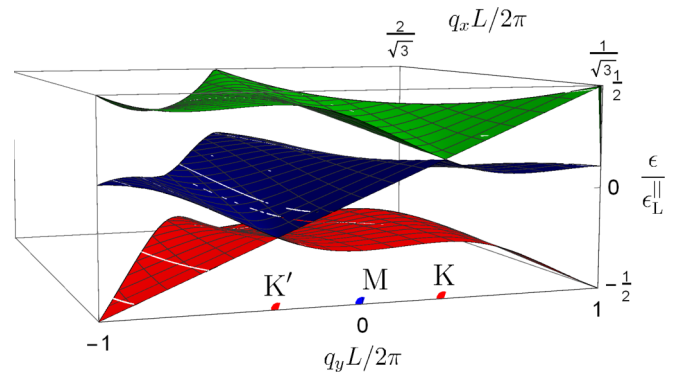

FIG. 1. Helical model band structure over half of the rhombic Brillouin zone (BZ) defined in Fig. 3(c). The bands in the other half of the BZ can be obtained by the reflection. The model's band energies ϵ_q^{n0} are given by Eq. (11) and depend on a single controlling parameter α which was set to $\alpha = 1.1$ in this illustration. The bands touch at Dirac points located at high-symmetry K, K', and Γ points.
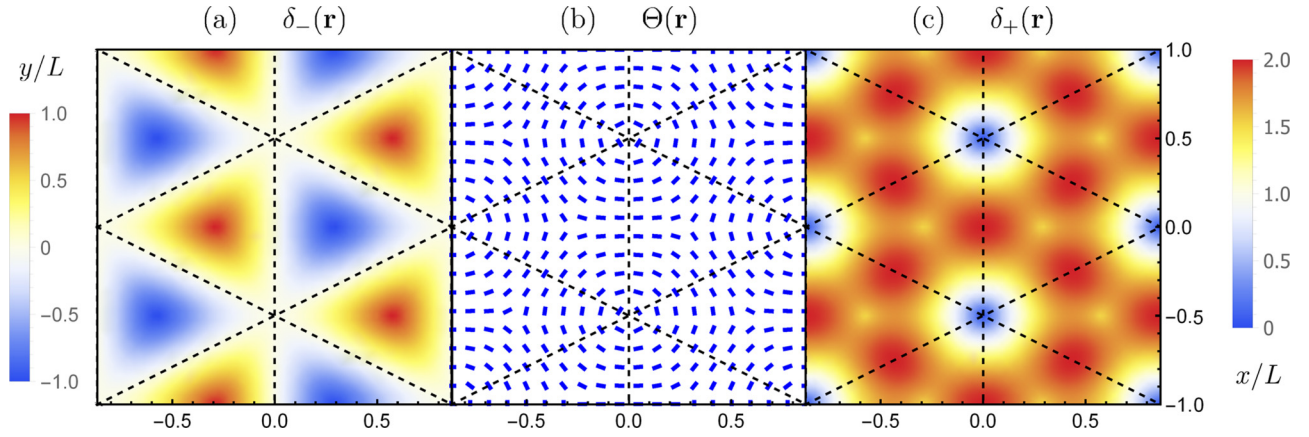
FIG. 2. Spatial distribution of the the gap parameters in Eq. (4): (a) the gap minimum δ_-; (b) the angle $\theta(\mathbf{r})$ which specifies the direction in momentum space at which minima are achieved; (c) the gap maximum δ_+. The dashed lines highlight the network of domain walls that separate regions in which the hybridization is dominated by T_{AB} from regions in which it is dominated by T_{BA}.

independent, while electronic states in two valleys K and K' transform to each other by the time-reversal transformation. The sublattice-dependent interlayer hopping operator is given by

$$T(\mathbf{r}) = \frac{w}{3} \sum_{i=1}^{3} e^{-i\mathbf{k}_i \mathbf{r}} T_i, \qquad (2)$$

where w is a hybridization energy scale. The vectors $\mathbf{k}_1 = -k_\theta \mathbf{e}_y$, $\mathbf{k}_{2,3} = k_\theta(\pm\sqrt{3}\mathbf{e}_x + \mathbf{e}_y)/2$ all have magnitude equal to the twist-induced separation between the Dirac points of the two layers, $k_\theta = 2k_D \sin(\theta/2)$ where $k_D = 4\pi/3a_0$ is the magnitude of the Brillouin-zone corner vector of a single layer and a_0 is the corresponding Bravais period. The matrices T_i are given by

$$T_1 = \begin{pmatrix} 1 & 1 \\ 1 & 1 \end{pmatrix}, \quad T_2 = \begin{pmatrix} e^{-i\zeta} & 1 \\ e^{i\zeta} & e^{-i\zeta} \end{pmatrix}, \quad T_3 = \begin{pmatrix} e^{i\zeta} & 1 \\ e^{-i\zeta} & e^{i\zeta} \end{pmatrix},$$

with $\zeta = 2\pi/3$. The diagonal matrix elements of the hopping operator are identical, $T_{AA} = T_{BB} \equiv T_d$, and correspond to tunneling between atoms on the same sublattice, while the off-diagonal matrix elements T_{AB} and T_{BA} correspond to the tunneling between opposite sublattices. Their spatial dependence is periodic with the period of the moiré pattern $L = a_0/[2\sin(\theta/2)]$.

The network model we derive has its widest range of applicability in the large gate voltage regime $\epsilon_L \ll u \sim w$ where $\epsilon_L = 2\pi\hbar v/L$ is the energy scale of the network minibands, as we explain below. When hybridization is neglected the conduction band of the low-potential top layer and the valence band of the high-potential bottom layer intersect on a circle of radius $p_u = u/v$. After projection of the full four-band Hamiltonian (1) to these bands we find that

$$H = \begin{pmatrix} v(p - p_u) & t_P + t_S \\ t_P^* + t_S^* & -v(p - p_u) \end{pmatrix}, \qquad (3)$$

where $v(p - p_u)$ is the isolated conduction band dispersion of the top layer and $-v(p - p_u)$ is the valence band dispersion of the bottom layer. In Eq. (3) we have separated the tunneling matrix element into two parts: an anisotropic part

with p-wave symmetry $t_P(\phi_\mathbf{p}, \mathbf{r}) = [T_{BA} e^{-i\varphi_\mathbf{p}} - T_{AB} e^{i\varphi_\mathbf{p}}]/2$, where $\varphi_\mathbf{p}$ is the direction of a momentum $\mathbf{p}$, and an isotropic part $t_S(\mathbf{r}) = -i T_d(\mathbf{r}) \sin(\theta/2)$ independent of $\varphi_\mathbf{p}$ that can be neglected [49] for $\theta \ll 1$. The resulting local spectrum $\epsilon_{\mathbf{p}\pm} = \pm\sqrt{(vp - u)^2 + \Delta_\mathbf{p}^2}$ has an anisotropic gap

$$\Delta_\mathbf{p}^2 = \delta_-^2 \cos^2[\varphi_\mathbf{p} - \Theta] + \delta_+^2 \sin^2[\varphi_\mathbf{p} - \Theta] \qquad (4)$$

which achieves minima $|\delta_-| = ||T_{AB}| - |T_{BA}||/2$ at momentum orientations $\varphi_I = \Theta$ and $\varphi_{II} = \Theta + \pi$, where $\Theta(\mathbf{r}) = (\arg[T_{BA}] - \arg[T_{AB}])/2$. The gap is maximized at $\delta_+(\mathbf{r}) = (|T_{BA}| + |T_{AB}|)/2$ at the two perpendicular orientations. The spatial distributions of these quantities are illustrated in Fig. 2 where the domain walls clearly appear as a change in sign of δ_-.

It follows from the preceding analysis that the gap in the local electronic spectrum (4) closes if $|T_{AB}| = |T_{BA}|$. This condition is satisfied along the domain walls specified by dashed lines in Fig. 2(a), where we illustrate the spatial pattern of $\delta_-(\mathbf{r})$. The domain walls separate regions where the interlayer hybridization is dominated by the T_{AB} from regions in which it is dominated by T_{BA}. The local valley Chern number of Hamiltonian (3)

$$C = \int \frac{d\mathbf{p}}{4\pi} \mathbf{d} \left[\frac{\partial \mathbf{d}}{\partial p_x} \times \frac{\partial \mathbf{d}}{\partial p_y} \right] = \frac{\delta_-}{|\delta_-|}, \qquad (5)$$

where $\mathbf{d} = \mathbf{h}/h$ and the vector $\mathbf{h}$ is defined by the Pauli matrix expansion of Eq. (3), $H = (\boldsymbol{\sigma} \cdot \mathbf{h})$. The local approximation for the electronic structure calculates local quantities from the local continuum model band Hamiltonian, and the corresponding momentum space integration is therefore over the full momentum space, and not over the Brillouin zone of the moiré pattern. The valley Chern number difference across the domain wall is $C_{AB} - C_{BA} = 2$, guaranteeing that two helical electronic channels are present in the gaps per valley and per spin.

In the vicinity of each domain wall the low-energy states are concentrated around the minima located at orientations $\varphi_{I(II)}$, which are perpendicular to the domain wall as illustrated in Fig. 2(b). By expanding the Hamiltonian (3) in the vicinity

of these minima, making a unitary transformation to place the mass terms on the diagonal, we are able to write the Hamiltonian as the sum of two identical anisotropic Dirac cones with the spatially dependent mass $\delta_-(r_\perp)$:

$$H_D = \begin{pmatrix} \delta_-(r_\perp) & v\hat{p}_\perp - iv_\parallel \hat{p}_\parallel \\ v\hat{p}_\perp + iv_\parallel \hat{p}_\parallel & -\delta_-(r_\perp) \end{pmatrix}. \qquad (6)$$

Here we have promoted the momenta to be operators, letting $p \to p_u + \hat{p}_\perp$ and $\delta_+\phi_{\mathbf{p}} \to v_\parallel \hat{p}_\parallel$. The velocity for momenta $\hat{p}_\perp$ perpendicular to the domain wall is the single-layer graphene Dirac velocity v. The velocity for momenta $\hat{p}_\parallel$ along the domain wall and Dirac mass $\delta_-(r_\perp)$ are approximated by their values at the domain wall center as follows:

$$v_\parallel = \frac{\delta_+}{p_u} \approx \frac{2wv}{3u}, \quad \delta_- \approx \sqrt{3}w \, \sin\left(\frac{2\pi r_\perp}{\sqrt{3}L}\right). \qquad (7)$$

Each Dirac point carries one half of the valley Chern number $C_D = \delta_-/2|\delta_-|$, and is responsible for a single helical state. The Dirac mass $\delta_-(\mathbf{r})$ changes sign across the domain wall and Eq. (6) therefore has a Jackiw-Rebbi [50] solution that describes helical electronic states with dispersion $\epsilon_{p_\parallel} = v_\parallel p_\parallel$, and wave function up to the normalization factor is given by

$$\psi_{p_\parallel}(r_\perp) = \begin{pmatrix} 1 \\ i \end{pmatrix} \exp\left[i\frac{p_\parallel r_\parallel}{\hbar} - \frac{wL}{\pi\hbar v}\sin^2\left(\frac{\pi r_\perp}{\sqrt{3}L}\right) \right]. \qquad (8)$$

The center of the AB/BA region, where wave functions of helical states from different domain walls overlap, are distanced at length $r_\perp^0 = L/2\sqrt{3}$ from them. The domain wall network is well developed if the overlap of wave functions $|\psi_{p_\parallel}(r_\perp^0)|^2|/|\psi_{p_\parallel}(0)|^2 = \exp[-w/\epsilon_L] \ll 1$ is weak. Here $\epsilon_L = 2\pi\hbar v/L$ is the character energy scale of the moiré pattern.

These helical states are the only electronic degrees of freedom present when $|\epsilon| \ll u, w$. Three sets of parallel domain walls with orientations differing by 120° surround AB and BA regions and intersect at a set of points with local AA stacking. The considerations we have discussed to this point establish the physical picture we use to motivate our phenomenological helical network model for domain wall states.

III. PHENOMENOLOGICAL NETWORK MODEL

Our phenomenological helical network model consists of the links and nodes illustrated in Figs. 3(a) and 3(b), which connect to form the domain wall pattern. We assume ballistic propagation along links and scattering only at nodes. The dispersion law along links, $\epsilon_q = v_\parallel q$, is consistent with the Jackiw-Rebbi confined mode solution. For $\epsilon_L \ll w \lesssim u$, the two Dirac cones on opposite sides of the ring at φ_I and φ_{II} are well separated in momentum space, allowing scattering between them to be neglected. This simplification allows us to consider a network with a single helical channel per link.

The full domain wall network can be constructed by placing the set of three elementary nodes on a triangular lattice
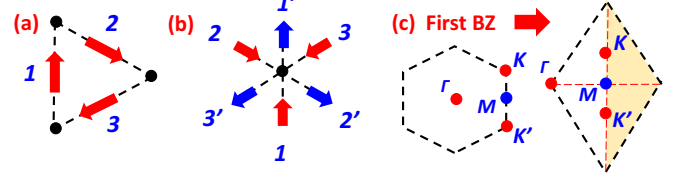

FIG. 3. (a) Elementary cell of the network. The wave-function amplitudes, links 1, 2, and 3, are denoted by $\psi_{ij} = \{\psi_{ij}^1, \psi_{ij}^2, \psi_{ij}^3\}$. (b) Node with three incoming and three outgoing channels characterized by the scattering matrix $\hat{S}$. (c) First Brillouin zone of the network in hexagonal and rhombohedral representations.

with elementary lattice vectors $\mathbf{l}_{1,2} = L(\pm\sqrt{3}\mathbf{e}_x + \mathbf{e}_y)/2$. The wave-function amplitudes on links 1, 2, and 3 of the cell centered at $\mathbf{R}_{ij} = i\mathbf{l}_1 + j\mathbf{l}_2$ are illustrated in Fig. 3(a) and denoted by $\psi_{ij} = \{\psi_{ij}^1, \psi_{ij}^2, \psi_{ij}^3\}$. Each node has three input and three output channels and therefore has a 3×3 unitary scattering matrix $\hat{S}$ whose detailed form depends in a complex way [51] on the spatial profile of the domain walls intersection. We follow a simpler phenomenological approach. By observing that the straightforward scattering amplitude magnitudes $|S_{11}| = |S_{22}| = |S_{33}|$ and the 240° deflection scattering amplitudes $|S_{12}| = |S_{13}| = |S_{21}| = |S_{23}| = |S_{31}| = |S_{32}|$ must be equal due to symmetry, it follows that the unitary matrix T can be parametrized by an angle α ranging between 0 and $\alpha_M = \arccos[1/3]$, and six phases $\phi_S, \phi_1^R, \phi_1^L, \phi_2^R, \phi_2^L, \phi_3$ ranging between 0 and 2π: $S = e^{i\phi_T}S_\phi^L \bar{S}S_\phi^R$, where ϕ_S is the average phase shift; $S_\phi^L = \text{diag}[e^{i(\phi_2^R + \phi_1^R + \phi_3)}, e^{-i\phi_2^L}, e^{-i\phi_1^L}]$ and $S_\phi^R = \text{diag}[e^{i(\phi_2^L + \phi_1^L - \phi_3)}, e^{-i\phi_2^R}, e^{-i\phi_1^R}]$ are phase shifts before and after scattering, which are not independent, and $\bar{S}$ is the unitary matrix:

$$\bar{S} = \begin{pmatrix} \cos(\alpha)e^{i\chi} & \frac{\sin(\alpha)}{\sqrt{2}} & \frac{\sin(\alpha)}{\sqrt{2}} \\ \frac{\sin(\alpha)}{\sqrt{2}} & -\frac{1+\cos(\alpha)e^{-i\chi}}{2} & \frac{1-\cos(\alpha)e^{-i\chi}}{2} \\ \frac{\sin(\alpha)}{\sqrt{2}} & \frac{1-\cos(\alpha)e^{-i\chi}}{2} & -\frac{1+\cos(\alpha)e^{-i\chi}}{2} \end{pmatrix}. \qquad (9)$$

Here $\chi = \arccos[\{3\cos^2(\alpha) - 1\}/2\cos(\alpha)]$. The electron flow conservation requires $P_f + 2P_d = 1$, where $P_f = \cos^2(\alpha)$ and $P_d = \sin^2(\alpha)/2$ are probabilities of an electron to be scattered to forward and two symmetric deflected channels. They are parametrized only by the angle α and are independent of scattering phases.

To find the electronic spectrum of the network we follow the transfer matrix approach. The outgoing ψ_{out} and incoming ψ_{in} electronic waves with energy ϵ at any node are connected by $\psi_{\text{out}} = e^{-i\phi_E}\hat{S}\psi_{\text{in}}$, where $\psi_{\text{out}} = (\psi_{i+1,j}^1, \psi_{i,j-1}^2, \psi_{i,j}^3)$ and $\psi_{\text{in}} = (\psi_{i,j-1}^1, \psi_{i,j}^2, \psi_{i+1,j}^3)$. Here $\phi_E = \epsilon L/\hbar v_\parallel$ is the dynamical phase accumulated by electrons while propagating between links. Bloch's theorem connects wave function amplitudes in different cells by $\psi_{ij} = e^{i\mathbf{q}\mathbf{R}_{ij}}\bar{\psi}$, where $\bar{\psi} \equiv \{\bar{\psi}^1, \bar{\psi}^2, \bar{\psi}^3\}$ and $\mathbf{q}$ is the moiré momentum. The connection between input and output waves can be rewritten as $[\lambda - U_{\mathbf{q}}]\bar{\psi} = 0$, and has a nontrivial solution only if $\lambda = e^{i(\phi_E - \phi_T)}$ is equal to one of the

eigenvalues of the matrix

$$
U_{\mathbf{q}} = \begin{pmatrix}
\cos\alpha\, e^{i(\chi+\phi_1^R+\phi_2^R+\phi_1^L+\phi_2^L-\mathbf{q}\mathbf{l}_1-\mathbf{q}\mathbf{l}_2)} & \frac{\sin\alpha}{\sqrt{2}} e^{i(\phi_1^R+\phi_3-\mathbf{q}\mathbf{l}_1)} & \frac{\sin\alpha}{\sqrt{2}} e^{i(\phi_2^R+\phi_3)} \\
\frac{\sin\alpha}{\sqrt{2}} e^{i(\phi_1^L-\phi_3)} & -\frac{1+\cos\alpha\, e^{-i\chi}}{2} e^{i(\mathbf{q}\mathbf{l}_2-\phi_2^R-\phi_2^L)} & \frac{1-\cos\alpha\, e^{-i\chi}}{2} e^{i(\mathbf{q}\mathbf{l}_1+\mathbf{q}\mathbf{l}_2-\phi_1^R-\phi_2^L)} \\
\frac{\sin\alpha}{\sqrt{2}} e^{i(\phi_2^L-\phi_3-\mathbf{q}\mathbf{l}_2)} & \frac{1-\cos\alpha\, e^{-i\chi}}{2} e^{-i(\phi_2^R+\phi_1^L)} & -\frac{1+\cos\alpha\, e^{-i\chi}}{2} e^{i(\mathbf{q}\mathbf{l}_1-\phi_1^R-\phi_1^L)}
\end{pmatrix}. \tag{10}
$$

It should be noted that the network spectrum can be approached within the discrete evolution method [46], and the matrix $U_{\mathbf{q}}$ plays the role of the discrete evolution operator. Its three eigenvalues $\lambda_{\mathbf{q}}^n$ are labeled by $n = -1, 0, 1$ and correspond to three bands that periodically repeat with energy $\epsilon_L^{\parallel} = 2\pi\hbar v_{\parallel}/L$ and are given by

$$
\epsilon_{\mathbf{q}}^{nm} = \epsilon_L^{\parallel}\left(\frac{\arg[\lambda_{\mathbf{q}}^n]}{2\pi} + \frac{\phi_T}{2\pi} + m\right). \tag{11}
$$

The phase ϕ_T just results in a rigid shift of all bands in energy, while m is an integer and ensures their periodicity. The energy periodicity of the electronic structure is a feature of network models that distinguishes them from standard tight-binding models.

Since the matrix $U_{\mathbf{q}}$ is also unitary $U_{\mathbf{q}}^+ = U_{\mathbf{q}}^{-1}$ and $\det[U_{\mathbf{q}}] = 1$, its eigenvalue problem can be written in a compact way:

$$
\lambda_{\mathbf{q}}^3 - \text{tr}[U_{\mathbf{q}}]\lambda_{\mathbf{q}}^2 + \text{tr}[U_{\mathbf{q}}^+]\lambda_{\mathbf{q}} - 1 = 0. \tag{12}
$$

The electronic spectrum therefore depends only on the trace of the matrix $U_{\mathbf{q}}$ that is given by

$$
\text{tr}[U_{\mathbf{q}}] = \cos(\alpha)e^{i\chi}e^{i(\Phi_1+\Phi_2-\mathbf{q}\mathbf{l}_1-\mathbf{q}\mathbf{l}_2)}
$$
$$
- \tfrac{1}{2}[1+\cos(\alpha)e^{-i\chi}][e^{i(\mathbf{q}\mathbf{l}_1-\Phi_1)} + e^{i(\mathbf{q}\mathbf{l}_2-\Phi_2)}]. \tag{13}
$$

Here we have introduced phases $\Phi_1 = \phi_1^L + \phi_1^R$, $\Phi_2 = \phi_2^L + \phi_2^R$. These phases Φ_1 and Φ_2 can be eliminated by the shift of the momentum space origin, and therefore do not influence the density of states of the network and electronic transport through it. The latter remarkably depend *only* on α, which in turn characterizes the distribution of scattering probability between forward and deflected channels.

It has been numerically shown [14] that, contrary to classical intuition, because nearby paths have a larger wave-function overlap with the incoming electron, deflection is the more likely outcome. For the presentation of results we chose $\alpha = 1.1$ corresponding to probabilities $P_f \approx 0.2$ and $P_d \approx 0.4$. We also use the set of phases $\phi_T = \Phi_1 = \Phi_2 = (\pi - 2\arcsin[3\sin\alpha/2\sqrt{2}])/3$ that ensures the discrete rotational symmetry of the network in respect to $120°$ around any node.

The first Brillouin zone of the network has a hexagonal shape and is illustrated in Fig. 3(c) where we also illustrate an equivalent rhombic primitive cell. The spectrum has the mirror symmetry across the KK' line since $\text{tr}[U_{\mathbf{q}_M-q_x,q_y}] = \text{tr}[U_{\mathbf{q}_M+q_x,q_y}]$, where $\mathbf{q}_M = 2\pi\mathbf{e}_x/\sqrt{3}L$ is the position of the M point in the Brillouin zone. A single period $\epsilon_{\mathbf{q}}^{n0}$ of the repeating band structure is plotted in the half of the rhombic Brillouin zone in Fig. 1, where we see that it is gapless because of Dirac band-touching points situated in Γ, K, and K' high-symmetry points. They are separated by momentum $\Delta k_D = 4\pi/3L$ and

energy $\Delta\epsilon_D = \epsilon_L^{\parallel}/3$. The density of states of the network is presented in Fig. 4 and is periodic with period $\Delta\epsilon_D$. It is three times smaller than the period of the network band structure $\epsilon_L^{\parallel}$, which reflects the symmetry between three links in an elementary cell of the model. The single period contains one zero at the Dirac point, and one saddle-point logarithmic divergence. The latter reflects the van Hove singularity due to the presence of saddle points in the network band structure, which are clearly visible in Fig. 1.

The gapless nature of the electronic spectrum of the network originates from its triangular symmetry. The momenta and energies of Dirac points are independent on α. Really, the discriminant $D = 27 + 4\text{tr}[U_{\mathbf{q}}]^3 + \text{tr}[U_{\mathbf{q}}^+]^3 - 18|\text{tr}[U_{\mathbf{q}}]|^2 - |\text{tr}[U_{\mathbf{q}}]|^4 = 0$ of the cubic eigenvalue problem (12) vanishes in Γ, K, and K' high-symmetry points for any α. Moreover the Dirac velocity in the vicinity of these points $v_D = v_{\parallel}/2$ is also α independent. The latter determines the positions and strength of van Hove singularities of the network density of states.

IV. DISCUSSIONS

The helical network model proposed here describes the electronic structure of twisted bilayer graphene in the regime of small twist angles and large strong displacement field. Recently it has been argued that there is a separate regime in graphene bilayers that can also be described as a honeycomb lattice network model [52]. In that case the network is not helical and
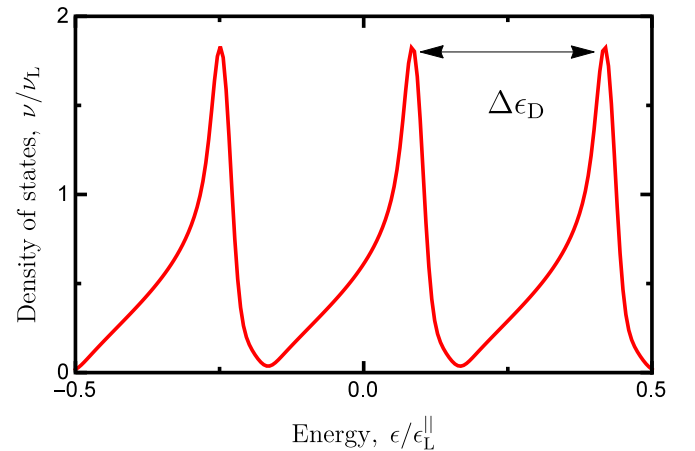
FIG. 4. The energy dependence of the density of states $\nu(\epsilon)$ per valley, spin and per Dirac point in the ring. It has three dips and three maxima separated from each other by $\Delta\epsilon_D = \epsilon_L^{\parallel}/3$. The primer correspond to Dirac points, while the latter to saddle points of the moiré pattern band structure presented in Fig. 1. The corresponding scale for the density of states is $\nu_L = \sqrt{3}\pi/\epsilon_L^{\parallel}L^2$.

does not require a displacement field, and is dependent instead on a special large twist angle close to commensuration.

Previous numerical calculations have addressed the electronic properties of twisted bilayer graphene in the same regime studied here [43], and have discovered a set of sharp features in the density of states which are nearly periodic in energy. For the case of twist angle $\theta = 0.2°$ and potential difference between layers $2u \approx 180$ meV, the numerical features are separated by $\Delta\epsilon_D \approx 21$ meV. Because the circumstance studied numerically are not fully in the regime in which our network model applies, our expressions for $v_\parallel$ do not apply. If we make the approximation $v_\parallel \approx v$, we find $\Delta\epsilon_D \approx \epsilon_L/3 \approx 20$ meV, in good agreement with the numeral calculations. Although further numerical work is necessary to fully test our theory, this comparison does seem to suggest that it provides an explanation for the unexpected set of density-of-states peaks in Ref. [43].

In a recent experiment [42] a small twist angle $\theta = 0.245°$ has been applied between layers to produce moiré patterns with period $L \approx 58$ nm. The resulting energy scale of the pattern $\epsilon_L = 2\pi\hbar v/L \approx 72$ meV is comparable with the gap induced by the applied displacement field, $\epsilon_g \approx 60$ meV. Again our model, which predicts a periodic set of density-of-states peaks, is not fully applicable. At this relatively small displacement field, only one density-of-states feature has been observed within the gap [42]. For the largest gaps $\epsilon_g \approx 250$ meV achievable in bilayer graphene [53,54], our model applies over a wide range of energies. Using the hybridization energy $w = 400$ meV [1] we estimate that the velocity of helical states $v_\parallel = 1.6 \times 10^6$ m/s is larger than the velocity of electrons in graphene $v = 10^6$ m/s. The period of the network is equal to $\epsilon_L^\parallel \approx 115$ meV and the period of the density of states $\Delta\epsilon_D \approx 38$ meV. Because the density of states period is much smaller than the gap, we expect a set of features due to van Hove singularities of network spectrum to be well resolved in experiments. Alternatively, the condition $\epsilon_L^\parallel \ll \epsilon_g$ can be achieved at smaller twist angles θ.

The electronic band structure of twisted graphene bilayer in the absence of a displacement field is very sensitive to a twist angle θ, with vanishing Dirac velocities and flat moiré bands emerging at a set of magic angles [20]. We predict that magic angle behavior is absent at strong displacement fields. Instead, the only low-energy degrees of freedom are helical states propagating along domain walls separating regions of different stacking. When the domain wall network is well developed the low-energy part of its band structure is universal and weakly depends on θ, apart from the twist-angle dependence of the energy scale ϵ_L.

To conclude, we have introduced a phenomenological network model that captures the electronic structure of twisted bilayer graphene with a large displacement field in the energy range below the AB and BA gaps where only topologically confined domain wall states are present. Motivated by the recent observation of the domain wall network in scanning tunneling microscopy experiments [42] we have focused on its band structure and density of states. Very recently, signatures of the network formation have been found in magnetotransport experiments [55], which can be addressed theoretically using the model developed in this work.

[1] E. McCann and M. Koshino, Rep. Prog. Phys. **76**, 056503 (2013).

[2] A. Rozhkov, A. Sboychakov, A. Rakhmanov, and F. Nori, Phys. Rep. **648**, 1 (2016).

[3] I. Martin, Y. M. Blanter, and A. F. Morpurgo, Phys. Rev. Lett. **100**, 036804 (2008).

[4] A. S. Nunez, E. S. Morell, and P. Vargas, Appl. Phys. Lett. **98**, 262107 (2011).

[5] D. A. Cosma and V. I. Fal'ko, Phys. Rev. B **92**, 165412 (2015).

[6] D. R. da Costa, A. Chaves, S. H. R. Sena, G. A. Farias, and F. M. Peeters, Phys. Rev. B **92**, 045417 (2015).

[7] F. Zhang, A. H. MacDonald, and E. J. Mele, Proc. Natl. Acad. Sci. USA **110**, 10546 (2013).

[8] A. Vaezi, Y. Liang, D. H. Ngai, L. Yang, and E.-A. Kim, Phys. Rev. X **3**, 021018 (2013).

[9] M. Koshino, Phys. Rev. B **88**, 115409 (2013).

[10] L.-J. Yin, H. Jiang, J.-B. Qiao, and L. He, Nat. Commun. **7**, 11760 (2016).

[11] L. Ju, Z. Shi, N. Nair, Y. Lv, C. Jin, J. Velasco, Jr., C. Ojeda-Aristizabal, H. A. Bechtel, M. C. Martin, A. Zettl, J. Analytis, and F. Wang, Nature (London) **520**, 650 (2015).

[12] J. Li, K. Wang, K. J. McFaul, Z. Zern, Y. Ren, K. Watanabe, T. Taniguchi, Z. Qiao, and J. Zhu, Nat. Nanotechnol. **11**, 1060 (2016).

[13] Z. Qiao, J. Jung, Q. Niu, and A. H. MacDonald, Nano Lett. **11**, 3453 (2011).

[14] Z. Qiao, J. Jung, C. Lin, Y. Ren, A. H. MacDonald, and Q. Niu, Phys. Rev. Lett. **112**, 206601 (2014).

[15] H. Pan, X. Li, F. Zhang, and S. A. Yang, Phys. Rev. B **92**, 041404 (2015).

[16] A. R. Wright and T. Hyart, Appl. Phys. Lett. **98**, 251902 (2011).

[17] Y. Ren, J. Zeng, K. Wang, F. Xu, and Z. Qiao, Phys. Rev. B **96**, 155445 (2017).

[18] V. Mosallanejad, K. Wang, Z. Qiao, and G. Guo, arXiv:1704.01504.

[19] Y. Ren, Z. Qiao, and Q. Niu, Rep. Prog. Phys. **79**, 066501 (2016).

[20] R. Bistritzer and A. H. MacDonald, Proc. Natl. Acad. Sci. USA **108**, 12233 (2011).

[21] J. Jung, A. Raoux, Z. Qiao, and A. H. MacDonald, Phys. Rev. B **89**, 205414 (2014).

[22] A. V. Rozhkov, A. O. Sboychakov, A. L. Rakhmanov, and F. Nori, Phys. Rev. B **95**, 045119 (2017).

[23] D. Weckbecker, S. Shallcross, M. Fleischmann, N. Ray, S. Sharma, and O. Pankratov, Phys. Rev. B **93**, 035452 (2016).

[24] J. M. B. Lopes dos Santos, N. M. R. Peres, and A. H. Castro Neto, Phys. Rev. B **86**, 155449 (2012).

[25] J. M. B. Lopes dos Santos, N. M. R. Peres, and A. H. Castro Neto, Phys. Rev. Lett. **99**, 256802 (2007).

[26] J. C. W. Song, P. Samutpraphoot, and L. S. Levitov, Proc. Natl. Acad. Sci. USA **112**, 10879 (2015).

[27] M. Mucha-Kruczyński, J. R. Wallbank, and V. I. Fal'ko, Phys. Rev. B **93**, 085409 (2016).

[28] R. de Gail, M. O. Goerbig, F. Guinea, G. Montambaux, and A. H. Castro Neto, Phys. Rev. B **84**, 045436 (2011).

[29] G. Trambly de Laissardière, D. Mayou, and L. Magaud, Phys. Rev. B **86**, 125413 (2012).

[30] F. Gargiulo and O. V. Yazyev, 2D Mater. **5**, 015019 (2018).

[31] N. N. T. Nam and M. Koshino, Phys. Rev. B **96**, 075311 (2017).

[32] X. Bi, J. Jung, and Z. Qiao, Phys. Rev. B **92**, 235421 (2015).

[33] G. Chen, M. Sui, D. Wang, S. Wang, J. Jung, P. Moon, S. Adam, K. Watanabe, T. Taniguchi, S. Zhou, M. Koshino, G. Zhang, and Y. Zhang, Nano Lett. **17**, 3576 (2017).

[34] S. Dai, Y. Xiang, and D. J. Srolovitz, Nano Lett. **16**, 5923 (2016).

[35] P. San-Jose, R. V. Gorbachev, A. K. Geim, K. S. Novoselov, and F. Guinea, Nano Lett. **14**, 2052 (2014).

[36] V. Cherkez, G. T. de Laissardière, P. Mallet, and J.-Y. Veuillen, Phys. Rev. B **91**, 155428 (2015).

[37] Q. Yao, R. van Bremen, G. J. Slotman, L. Zhang, S. Haartsen, K. Sotthewes, P. Bampoulis, P. L. de Boeij, A. van Houselt, S. Yuan, and H. J. W. Zandvliet, Phys. Rev. B **95**, 245116 (2017).

[38] J. S. Alden, A. W. Tsen, P. Y. Huang, R. Hovden, L. Brown, J. Park, D. A. Muller, and P. L. McEuen, Proc. Natl. Acad. Sci. USA **110**, 11256 (2013).

[39] K. Kim, A. DaSilva, S. Huang, B. Fallahazad, S. Larentis, T. Taniguchi, K. Watanabe, B. J. LeRoy, A. H. MacDonald, and E. Tutuc, Proc. Natl. Acad. Sci. USA **114**, 3364 (2017).

[40] F. Hu, S. R. Das, Y. Luan, T.-F. Chung, Y. P. Chen, and Z. Fei, Phys. Rev. Lett. **119**, 247402 (2017).

[41] Y. Cao, V. Fatemi, S. Fang, K. Watanabe, T. Taniguchi, E. Kaxiras, and P. Jarillo-Herrero, Nature (London) **556**, 43 (2018).

[42] S. Huang, K. Kim, D. K. Efimkin, T. Lovorn, T. Taniguchi, K. Watanabe, A. H. MacDonald, E. Tutuc, and B. J. LeRoy, arXiv:1802.02999.

[43] P. San-Jose and E. Prada, Phys. Rev. B **88**, 121408 (2013).

[44] G. Trambly de Laissardière, O. F. Namarvar, D. Mayou, and L. Magaud, Phys. Rev. B **93**, 235135 (2016).

[45] J. T. Chalker and P. D. Coddington, J. Phys. C **21**, 2665 (1988).

[46] C.-M. Ho and J. T. Chalker, Phys. Rev. B **54**, 8708 (1996).

[47] V. V. Mkhitaryan and M. E. Raikh, Phys. Rev. B **79**, 125401 (2009).

[48] A geometry of the graphene bilayer needs to be characterized not only by a twist θ, but also by a relative translation vector **d**. As has been shown previously [20], the latter only shifts the moiré pattern, while its electronic band structure is independent on **d**.

[49] The isotropic contribution t_S is important only in the vicinity of domain wall intersections. In our phenomenological network model the scattering matrix for nodes T is parametrized in a phenomenological way and details of the intersections profile are of importance.

[50] R. Jackiw and C. Rebbi, Phys. Rev. D **13**, 3398 (1976).

[51] J. R. Anglin and A. Schulz, Phys. Rev. B **95**, 045430 (2017).

[52] H. K. Pal, S. Spitz, and M. Kindermann, arXiv:1803.07060.

[53] K. Kanayama and K. Nagashio, Sci. Rep. **5**, 15789 (2015).

[54] Y. Zhang, T.-T. Tang, C. Girit, Z. Hao, M. C. Martin, A. Zettl, M. F. Crommie, Y. R. Shen, and F. Wang, Nature (London) **459**, 820 (2017).

[55] P. Rickhaus, J. Wallbank, S. Slizovskiy, R. Pisoni, H. Overweg, Y. Lee, M. Eich, M.-H. Liu, K. Watanabe, T. Taniguchi, V. Fal'ko, T. Ihn, and K. Ensslin, arXiv:1802.07317.